Liquid Crystals
Publication details, including instructions for authors and subscription information:
http://www.informaworld.com/smpp/title~content=t713926090

Electric field-induced phase transitions in a smectic chiral liquid crystal

S. Essid[a]; N. Bitri[ab]; H. Dhaouadi[a]; A. Gharbi[a]; J. P. Marcerou[b]
[a] Laboratoire de Physique de la Matière Molle Faculté des Sciences de Tunis, El Manar TUNIS, Tunisie
[b] Centre de Recherches Paul Pascal, Pessac, France

To cite this Article Essid, S. , Bitri, N. , Dhaouadi, H. , Gharbi, A. and Marcerou, J. P.(2009) 'Electric field-induced phase transitions in a smectic chiral liquid crystal', Liquid Crystals, 36: 4, 359 — 364
To link to this Article: DOI: 10.1080/02678290902898182
URL: http://dx.doi.org/10.1080/02678290902898182

Liquid Crystals,
Vol. 36, No. 4, April 2009, 359–364

Taylor & Francis
Taylor & Francis Group

Electric field-induced phase transitions in a smectic chiral liquid crystal

S. Essid[a], N. Bitri[a,b]*, H. Dhaouadi[a], A. Gharbi[a] and J.P. Marcerou[b]

[a]*Laboratoire de Physique de la Matière Molle Faculté des Sciences de Tunis, 2092 El Manar TUNIS, Tunisie;* [b]*Centre de Recherches Paul Pascal, 115, Av. Albert-Schweitzer, 33600 Pessac, France*

(Received 18 December 2008; final form 16 March 2009)

The (*E–T*) phase diagram of the chiral smectic liquid crystal C7F2 has been established by varying the two thermodynamic parameters: temperature (*T*) and electric field (*E*). In its bulk state without field, the studied compound exhibits only the SmA, SmC^*_α and the SmC^*_A phases. These ground phases are transformed into the ferroelectric SmC* phase under high field with an intermediate ferrielectric phase appearing at lower field in the temperature range around the SmC^*_α to SmC^*_A phase transition.

Keywords: phase transitions; chirality; tilted smectic liquid crystal; phase diagram

1. Introduction

Chiral liquid crystals exhibiting the helicoidal smectic phases are of considerable interest, because of both their potential applications and their remarkable properties. They are distinguished by their unit cell where the number of layers varies from one to four. The SmC* phase is one example of ferroelectric, or more properly helielectric, liquid crystals: it has a unit cell of one layer. The SmC^*_A phase exhibits anticlinic order (alternating tilt direction in adjacent layers) (*1*, *2*) so that the unit cell has two layers. Other variations of the chiral smectic phases such as the SmC^*_α , SmC^*_{FI1} and SmC^*_{FI2}, differ in terms of their local order, with the same tilt inside the layers but a different distribution of the azimuthal angle φ with a periodicity of three (SmC^*_{FI1}), four (SmC^*_{FI2}) and more smectic layers for the SmC^*_α (see (*3*)).

If any of these phases is subject to a large enough applied field it will be converted into the unwound SmC* ferroelectric phase. Anyway it has been shown (*4*, *5*) that one may encounter at least an intermediate ferrielectric phase at lower fields.

In order to characterise the behaviour of a given compound under field, one has to plot a precise *T–E* (temperature–electric field) phase diagram. This has been done previously by several authors (*4–9*). To build such a diagram, one has to apply an electric field in the layer plane of an aligned smectic sample and measure some quantity that may be electric (polarisation, current, voltage) or optical (birefringence, intensity). To avoid possible misinterpretations, it appears that two conditions have to be fulfilled.

- The phase sequence and the transition temperatures at zero electric field ($E = 0$ V) must be the same as determined in the bulk, for example by polarising optical microscopy (POM) and differential scanning calorimetry (DSC; ground phase sequence). This problem has been encountered in the very first phase diagram of MHPOBC (*9*) where it was shown that in a thin planar sample, the SmC^*_{FI1} ground phase is replaced by a mixture of SmC* and SmC^*_A.
- The boundaries in the diagram must correspond to phase transitions and not to reorientations or rearrangements of the director in a single phase. Some examples of such a behaviour would be the Fredericks transition (*10*) or the bistable anchoring (*11*, *12*) in nematics.

We report here on the study of the chiral smectic liquid crystal C7F2 exhibiting for the ground sequence the SmA, SmC^*_α and SmC^*_A phases. It has been chosen for its relatively large SmC^*_α range and because it is not subject to demixing in the thin planar sample. Our experimental results will be compared later with the (*E–T*) phase diagram obtained with a photo-elastic modulator (PEM) technique by Orihara *et al.* (*4*) in the MHPOCBC compound which has the same phase sequence.

2. Experimental details

2.1 Material

The investigated compound C7F2 was synthesised by Nguyen *et al.* (*13*). The chemical structure of the compound is given in Figure 1. DSC (Perkin-Elmer DSC 7)

*Corresponding author. Email: bitri@crpp-bordeaux.cnrs.fr

ISSN 0267-8292 print/ISSN 1366-5855 online

DOI: 10.1080/02678290902898182
http://www.informaworld.com

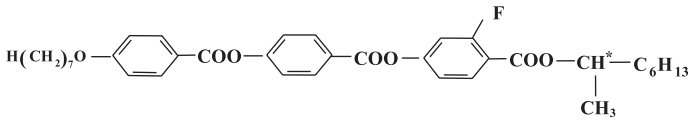

Figure 1. Chemical formula of C7F2 compound.

and texture observations with POM have revealed the following sequence (*13*):

$$\text{Cr}\ (59.4^\circ\text{C}) \rightarrow \text{SmC}_A^*\ (103.5^\circ\text{C}) \rightarrow \text{SmC}_\alpha^*\ (107.3^\circ\text{C}) \rightarrow \text{SmA}\ (144.5^\circ\text{C}) \rightarrow \text{Iso}.$$

2.2 Setup

To build up the phase diagram of the studied-compound, we used the electro-optic, the constant current and the dielectric spectroscopy methods. The cell used in the experiments is in the planar geometry. In a commercial cell with a thickness about 5.6 μm (EHC, Japan) the material was sandwiched in between ITO and polymer coatings for planar alignment. The active area was 25 mm^2. It made a capacitor at most 1 nF in series with a 2 kΩ resistor thus giving a cut-off frequency of a few 100 kHz for dielectric experiments.

Moreover, when a phase transition was found by checking the electrical response under bias field, we double checked it by monitoring the appearance of the sample in the polarising microscope (Olympus BM4).

2.2.1 Electro-optic studies

We apply a voltage which is periodic in time (frequency 40–50 Hz) and may have different shapes such as square wave, triangular or more complicated shapes. We record the signal on a Tektronix 340 oscilloscope. The current response is the sum of the charge of the cell capacitor, the ionic conductivity and a hump linked to the polarisation which reads

$$i_{p(t)} = \int_S dx\,dy \left(\frac{\partial P_z}{\partial t}\right) \tag{1}$$

and corresponds to the derivative versus time of the projection of the macroscopic polarisation P over the direction z of the applied field.

In the electro-optic investigations, the transitions to the unwound ferroelectric C^* phase were determined by measuring the threshold fields when applying a rectangular wave. It is defined as being the field from which the peak of polarisation appears or changes its amplitude suddenly. At low temperature ($T < 101^\circ$C) one sees only one direct phase transition to the unwound ferroelectric C^* with one unique threshold field. On the other hand, in the temperature range 101.5–103.5°C two threshold fields have been detected (Figure 2). We see two plateaux of polarisation denoting that the transition to the SmC* phase occurs via an intermediate phase, that we call Ferri (ferrielectric phase) with a macroscopic polarisation about $\frac{1}{4}$ of the SmC* polarisation as shown in Figure 2. In addition, we observe that the colour of the sample changes. Three colours have been clearly seen, from a light green SmC_A^*, then a dark green (Ferri) and finally the SmC* phase always yellowish.

Each time our electro-optic investigations give us a clear indication of a phase transition, mainly above the SmC_A^* phase, we took them into account in the drawing of the final (E, T) phase diagram.

2.2.2 Constant current method

A Keithley 6220 current source is used and the cell voltage is monitored by the oscilloscope. The cell containing the sample behaves like a capacitor. In practice, we record the cell voltage at a constant current of 5 nA, imposed to the cell at a given temperature. This method was presented for the first time by Marcerou *et al.* (*5*). The curves show that one recovers two kinds of responses.

Firstly linear increases versus time of the charge of the capacitor with a slope inversely proportional to the dielectric constant in a given phase:

$$E = \frac{V}{e} = \frac{it}{\epsilon_\perp S} \tag{2}$$

where e is the cell thickness, S is the active surface, i is the current, $\epsilon_\perp$ is the in-plane dielectric constant and t is time.

Second, one or two plateaux at constant voltage V_c with a duration Δt, corresponding to the onset of the new phase. Two pieces of information can be extracted, the value of the field at the phase transition and the value of the difference of polarisations between the two phases by

$$\Delta P = \frac{i\Delta t}{S}. \tag{3}$$

Figure 3 shows typical curves of the cell voltage versus time. At low temperature ($T < 101.5^\circ$C), a

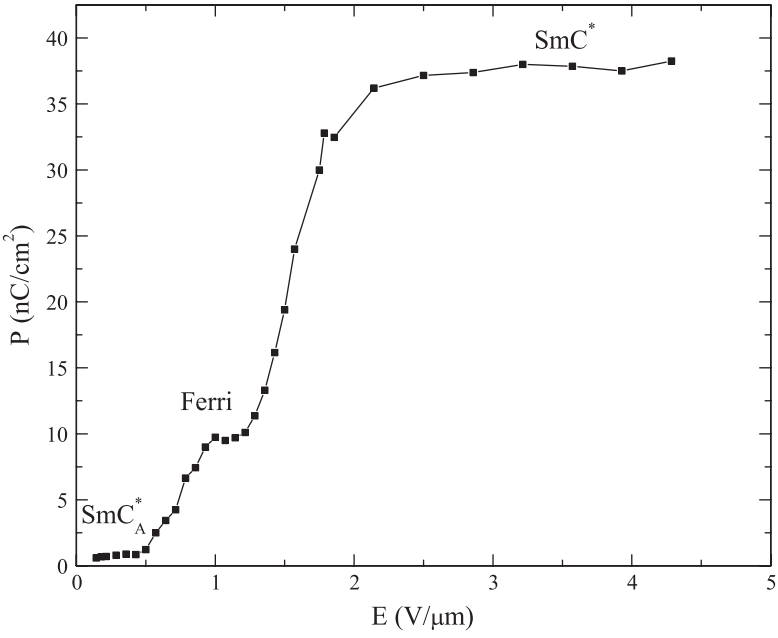

Figure 2. Field dependence of the polarisation for C7F2 at 102.8°C.

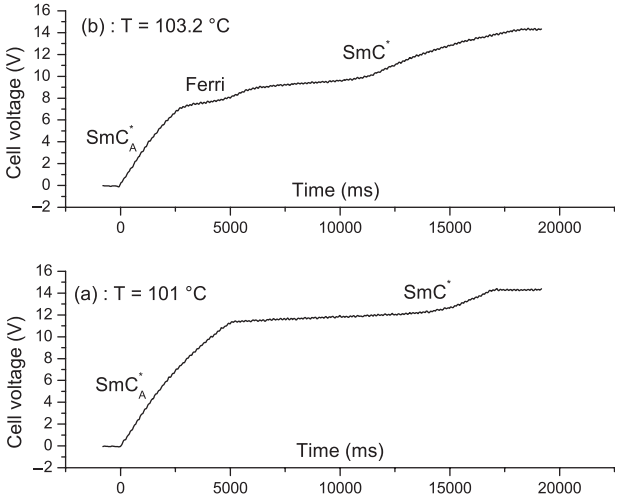

Figure 3. Typical curves showing the evolution of the cell voltage with time under a constant current of 5 nA. There is a monotonous increase inside a given phase mainly due to the charge of the capacitor, then one sees a plateau each time a first-order transition happens.

single plateau is seen which shows that the SmC_A^* phase transited directly to the unwound SmC* as seen in Figure 3(a). By increasing the temperature (in the range 101.5–103.8°C), we observe two successive plateaux which correspond to the phase transitions SmC_A^*–Ferri and Ferri-SmC*, respectively (Figure 3(b)). As the temperature further increases, the first plateau disappears so that at temperature slightly below the SmA–SmC_α^* transition, a single plateau is clearly seen again.

We only took into account the data where this behaviour with plateaux was unambiguous, corresponding clearly to first-order transitions between phases of different macroscopic polarisations. Furthermore we noted that, together with the plateaux, a stripped domain appears corresponding to the coexistence at the transition (*5*). Other behaviours with slope changes at a given point of the curve were not kept in order not to locate phase transitions where there could, in fact, be orientational changes. The last plateau is not relevant, it reflects only the upper voltage limit set for the generator.

The polarisations values determined in this way are compatible with those obtained by electro-optical method, in particular (Figure 3(b)) one finds again

$$P_{\text{Ferri}} = \frac{P_{\text{SmC*}}}{4}. \tag{4}$$

Our results confirm that electro-optic measurements and constant current method are particularly useful in the identification of first-order phase boundaries. However, the two methods alone are not sufficient to detect all transitions lines. Therefore, we performed in addition the dielectric investigation for the completion of the phase diagram.

2.2.3 *Dielectric spectroscopy*

In the dielectric spectroscopy setup, the voltage generator is a Philips PM 5192 delivering a static voltage up to 10 V together with the alternative modulation.

The in-phase and in-quadrature responses are given by a PAR 5301 lock-in amplifier. After stabilising the temperature and applying a constant bias field, a small sinusoidal field of about 150 mV (rms) in the frequency range of 200 Hz-200 kHz was superimposed. The complex dielectric constant ϵ^* ($\epsilon^* = \epsilon' - j\epsilon''$) was measured. Most of the time there is only one relaxation mode of the Debye kind due to the electroclinic effect (soft mode of the SmA to SmC phase transition) (*14*):

$$\epsilon'(\omega) = \epsilon_\infty + \frac{\epsilon_0 - \epsilon_\infty}{1 + \omega^2\tau^2} \tag{5}$$

$$\epsilon''(\omega) = \frac{(\epsilon_0 - \epsilon_\infty)\omega\tau}{1 + \omega^2\tau^2} \tag{6}$$

where ϵ' is the real part of the complex permittivity, ϵ'' gives the imaginary part, ω is the angular frequency of the applied field and ϵ_0 and ϵ_∞ are the static and the high-frequency dielectric permittivity, respectively.

The soft mode amplitude $\epsilon_0 - \epsilon_\infty$ and its relaxation time τ go through a maximum when crossing the SmA to SmC^*_α phase transition and the SmC^*_{el} to SmC* pseudo phase transition, as already reported in a similar compound (*5*).

Another lower-frequency mode, the Goldstone mode (*15*), could have been observed if there was a helielectric SmC* phase in the ground sequence where the macroscopic polarisation would be partially unwound by the electric field. This was not the case with the studied compound but we observed the onset of a new low-frequency relaxation below 200 Hz, at the value of the bias field where a phase transition was observed by the other techniques or at different values. The range of existence of this new mode was small, about ± 1 V in the bias voltage. The location of the maximum amplitude of this mode can be taken to identify a phase transition when it coincides with another criterion such as the voltage plateau or the field threshold in previous techniques or to the optical observations. The physical origin of this mode which appears together with the abrupt changes of the macroscopic polarisation lies probably in the high sensitivity to the field of the transient domains of the phase under construction.

3. Results

3.1 Phase sequence at zero field

The dielectric spectroscopy allows us to determine the ground phase sequence in the (E–T) plane. We perform a temperature scan of the dielectric constant ϵ without static field applied, as sketched in Figure 4. The dielectric constant is found to increase gradually

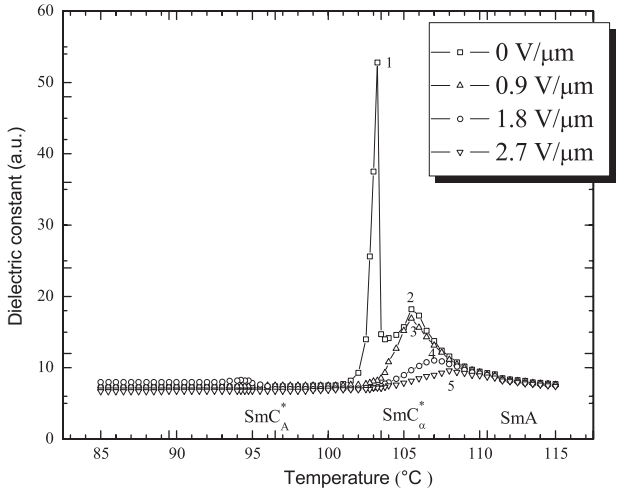

Figure 4. Dielectric response to an applied sinusoidal wave with f = 1 kHz at several dc bias electric fields for the C7F2 compound.

with decreasing temperature until the SmA–SmC^*_α transition is reached at the point marked 2 in the figure, at $T_{c_1} \sim 105.6$°C. This rather abrupt increase is the easiest way to determine the SmA–SmC^*_α phase transition which is hard to see with DSC. On further cooling, we distinguish at the point 1 a second very acute maximum of ϵ which corresponds to the SmC^*_α–SmC^*_A transition at $T_{c_2} \sim 103.2$°C.

As previously stated, the maximum of the response at T_{c_1} is due to the electroclinic effect while the peak at T_{c_2} is due to the new low-frequency mode. We follow the evolution of these peaks with respect to the bias field in order to sketch the missing phase boundaries in the (E, T) diagram.

3.2 Phase transitions under an applied electric field

The electroclinic peak at T_{c_1} shifts its position gradually toward higher temperature with the increase of the bias electric field from 0 to 2.7 V μm^{-1}. One can see that it keeps its shape for the point 3 at 1.6 V μm^{-1} while it becomes rounded for the last two maxima. Indeed the maxima (2, 3) and (4, 5) of the electroclinic peak correspond respectively to different points of the SmC^*_{el}–SmC^*_α and SmC^*_{el}–SmC* boundaries under electric field. As was done in a previous study (*5*), we performed careful scans of the temperature and bias field in order to sketch these two phase boundaries in the final diagram.

We note also that the second low-frequency mode at T_{c_2} is very sensitive to the bias field as it apparently disappears in Figure 4. In fact, if one scans the temperature and bias field with smaller steps, one sees a continuous evolution of the peak at T_{c_2} which is displaced towards higher temperatures when increasing

the bias. This allows us to draw the last transition line in the diagram that we identify as the SmC^*_α to Ferri phase transition.

4. Summary and discussion

By combining all of the experimental results we have successfully established the phase diagram of the C7F2 compound in the two-dimensional space involving the temperature and the applied electric field given in Figure 5. Its main characteristics is that it shows the onset of a ferrielectric domain with the shape of a down-under triangle above the SmC^*_α to SmC^*_A ground phase transition. At temperatures lower than in the ferrielectric domain, the SmC^*_A phase converts directly into the unwound SmC*. Above we recover the three phases region, SmC*–SmC^*_α–SmC^*_{el} already described in the C10F3 compound (*5*).

This diagram is similar to that established by Orihara *et al.* (*4*) in the MHPOCBC compound with the PEM technique, it has the same topology with a triangular domain in the middle that we identify with a ferrielectric phase in our case. However, we do not agree with the existence of so many tricritical points in the phase diagram. For us a tricritical point occurs when a phase transition between two and only two phases of different symmetry changes from first to second order. We observe with our compound that the remarkable points are always triple points where three different phases meet together. It seems that the PEM technique does not make enough difference between phase transitions and changes in the sample alignment. It is very surprising that with this technique, the birefringence of the sample under field is reported to be higher than the reference at the SmA to SmC^*_α transition. A perfectly aligned sample should have its maximum birefringence at this reference point.

Our results show that the transition under field from the ground tilted phases to the unwound ferroelectric SmC* phase occurs either with a direct transition or through an intermediate ferrielectric phase with non-zero spontaneous polarisation. We suggest that the theoretical model proposed by Hamaneh and Taylor (*16*) with a phase diagram involving only two phenomenological coefficients, could be adapted to take into account the polarisation and electric field effects. It seems possible to show that starting from a ground phase diagram, the ferrielectric SmC^*_{Fi1} and ferroelectric SmC* domain can grow under field and recover the other non-polar domains (*17*).

5. Conclusion

Experimental measurements as a function of temperature and the bias electric field have elucidated the ability of the different methods to investigate the existence of an induced phase and to established the phase diagram of the studied compound. In particular, it was found that all of the phase boundaries determined from the experiments corresponds to field-induced phase transition and not to reorientations in a single phase.

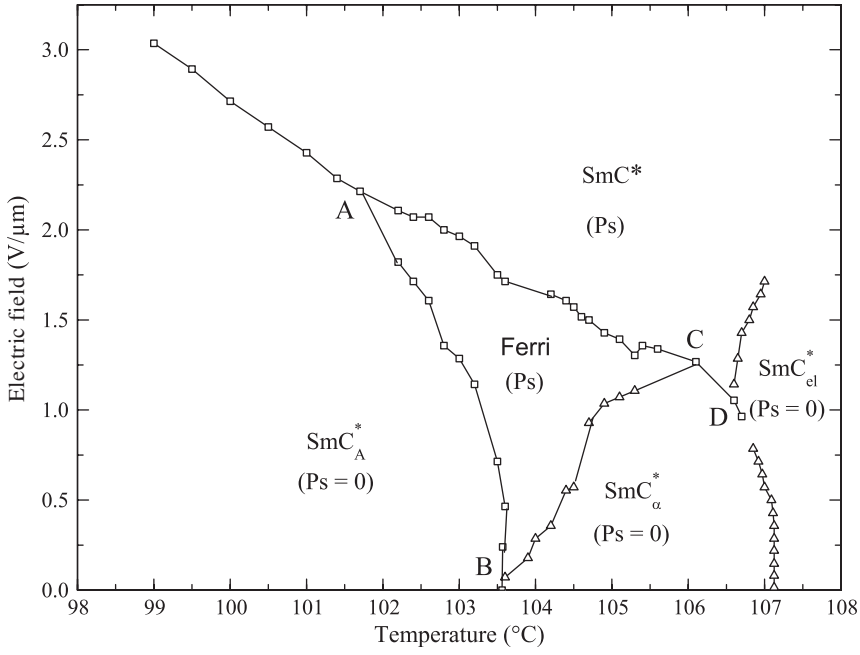

Figure 5. Final phase diagram where the different experimental results are put together.

Acknowledgements

We wish to acknowledge the support of CMCU and CNRS/DGRSRT contracts # 06/G1311. We also thank Huu Tinh Nguyen for synthesising the sample.

References

(1) Fukuda, A.; Takanishi, Y.; Isozaki, T.; Ishikawa, K.; Takezoe, H. *J. Mat. Chem.* **1994**, *4*, 997–1016.
(2) Galerne, Y.; Liebert, L. *Phys. Rev. Lett.* **1990**, *64*, 906–909.
(3) Mach, P.; Pindak, R.; Levelut, A.M.; Barois, P.; Nguyen, H.T.; Huang, C.C.; Furenlid, L. *Phys. Rev. Lett.* **1998**, *81*, 1015–1018.
(4) Orihara, H.; Naruse, Y.; Yagyu, M.; Fajar, A.; Uto, S. *Phys. Rev. E* **2005**, *72*, 040701(1)–040701(4).
(5) Marcerou, J.P.; Nguyen, H.T.; Bitri, N.; Gharbi, A.; Essid, S.; Soltani, T. *Eur. Phys. J. E* **2007**, *23*, 319–328.
(6) Manai, M.; Gharbi, A.; Essid, S.; Achard, M.F.; Marcerou, J.P.; Nguyen, H.T.; Rouillon, J.C. *Ferroelectrics* **2006**, *343*, 27–32.
(7) Hiraoka, K.; Chandani, A.D.L.; Gorecka, E.; Ouchi, Y.; Takezoe, H.; Fukuda, A. *Jpn. J. Appl. Phys* **1988**, *29*, L1473–L1476.
(8) Ghouddoussi, F.; Pantea, M.A.; Keyes, P.H.; Naik, P.; Vaishnava, P.P. *Phys. Rev. E* **2003**, *68*, 051706(1)–051706(8).
(9) Hatano, J.; Harazaki, M.; Sato, M.; Iwauchi, K.; Saito, S.; Murashiro, K. *Jpn. J. Appl. Phys* **1993**, *32*, 4344–4347.
(10) Fredericks, V.; Zolina, V. *Trans. Faraday Soc.* **1933**, *29*, 919–930.
(11) Barberi, R.; Durand, G. *Appl. Phys. Lett* **1991**, *58*, 2907–2909.
(12) Dozov, I.; Martinot-Lagarde, Ph.; Polossat, E.; Lelidis, I.; Giocondo, M.; Durand, G. *Proc. SPIE* **1997**, *61*, 61–69.
(13) Essid, S.; Manai, M.; Gharbi, A.; Marcerou, J.P.; Nguyen, H.T.; Rouillon, J.C. *Liq. Cryst.* **2004**, *31*, 1185–1193.
(14) Garoff, S.; Meyer, R.B. *Phys. Rev. Lett.* **1977**, *38*, 848–851.
(15) de Gennes, P.G.; Prost, J. *The Physics of Liquid Crystals*, second edition; Clarendon Press: Oxford, 1993.
(16) Hamaneh, M.B.; Taylor, P.L. *Phys. Rev. E* **2005**, *72*, 021706(1)–021706(9).
(17) H. Dhaouadi. PhD thesis (work in progress), 2009.